Supplementary Information

Testing with $\delta^{44/40}$Ca and $\delta^{88/86}$Sr for ocean acidification during the early Toarcian.

Q. Li[1,], J.M. McArthur[1,2], M.F. Thirlwall[1], A.V. Turchyn[3], K. Page[4], H.J. Bradbury[3], R. Weis[5] and D. Lowry[1]*

1. Earth Science, Royal Holloway University of London, Egham Hill, Egham, UK, TW20 0EX
2. Department of Earth Sciences, UCL, Gower Street, London WC1E 6BT, UK
3. Department of Earth Sciences, University of Cambridge, Cambridge, UK
4. University of Exeter, Penryn Campus, Penryn, Cornwall TR10 9FE,UK.
5. Palaeontological Department, National Museum of Natural History, 25 rue Münster, L-2160, Luxembourg, Grand-duchy of Luxembourg.

**Present address, Nu Instruments, Clywedog Road South, Wrexham, UK, LL13 9XS*
2. Corresponding author email: j.mcarthur@ucl.ac.uk

4.1. Sample preservation

Coherent trends of multiple palaeo-proxies through the studied interval, discussed briefly below, attest to the good preservation of the samples. The Peniche belemnites analyzed here are those used to prove the synchroneity of ammonite correlations between Peniche and Yorkshire (McArthur *et al.* 2020); the concordance of $^{87}Sr/^{86}Sr$ data between Peniche and Yorkshire (*ibid.*) provides compelling evidence of good preservation of analyzed samples. Discussions of preservation were presented in those papers. A more detailed study of Yorkshire samples in thin-section was made by McArthur *et al.* (2007) and a more comprehensive account of belemnite preservation can be found in Saelen *et al.* (1989) and Podlaha *et al.* (1998).

We assessed the degree of preservation/alteration of our samples by visual inspection of whole samples with the naked eye and with a hand lens, and inspection of fragmented samples by eye under the binocular microscope. For belemnites in hand specimen, the diagnostic features of good preservation are clarity of calcite and a brown colour in the range light to dark. The concentric rings typically seen in transverse section, and often termed 'growth rings', are faint or absent in well preserved belemnites. These bands are, in fact, rings caused by diagenetic alteration (Saelen *et al.* 1989). Alteration in belemnites is patchy, so even where alteration rings are abundant, the fragmented sample usually yields unaltered material. In fragmented samples picked for analysis, the diagnostic features of good preservation are a radial fabric, transparency, and little or no colour (Fig. S1). For brachiopods, one diagnostic feature of good preservation, arising from the decay of binding organic-matter, is a readiness of the fragmented sample to flake into thin sheets, and a readiness of those sheets to disintegrate into lath-like crystallites of uncoloured, clear, calcite (Fig. S1). Our samples show these features.

Our primary means of evaluating sample quality has been visual inspection under the microscope. Nevertheless, we note that the concentrations of Ca, Sr, Mg, and Na, and values of $\delta^{18}O$, in our samples (Table 1) are within the range of well-preserved biogenic calcites reported in

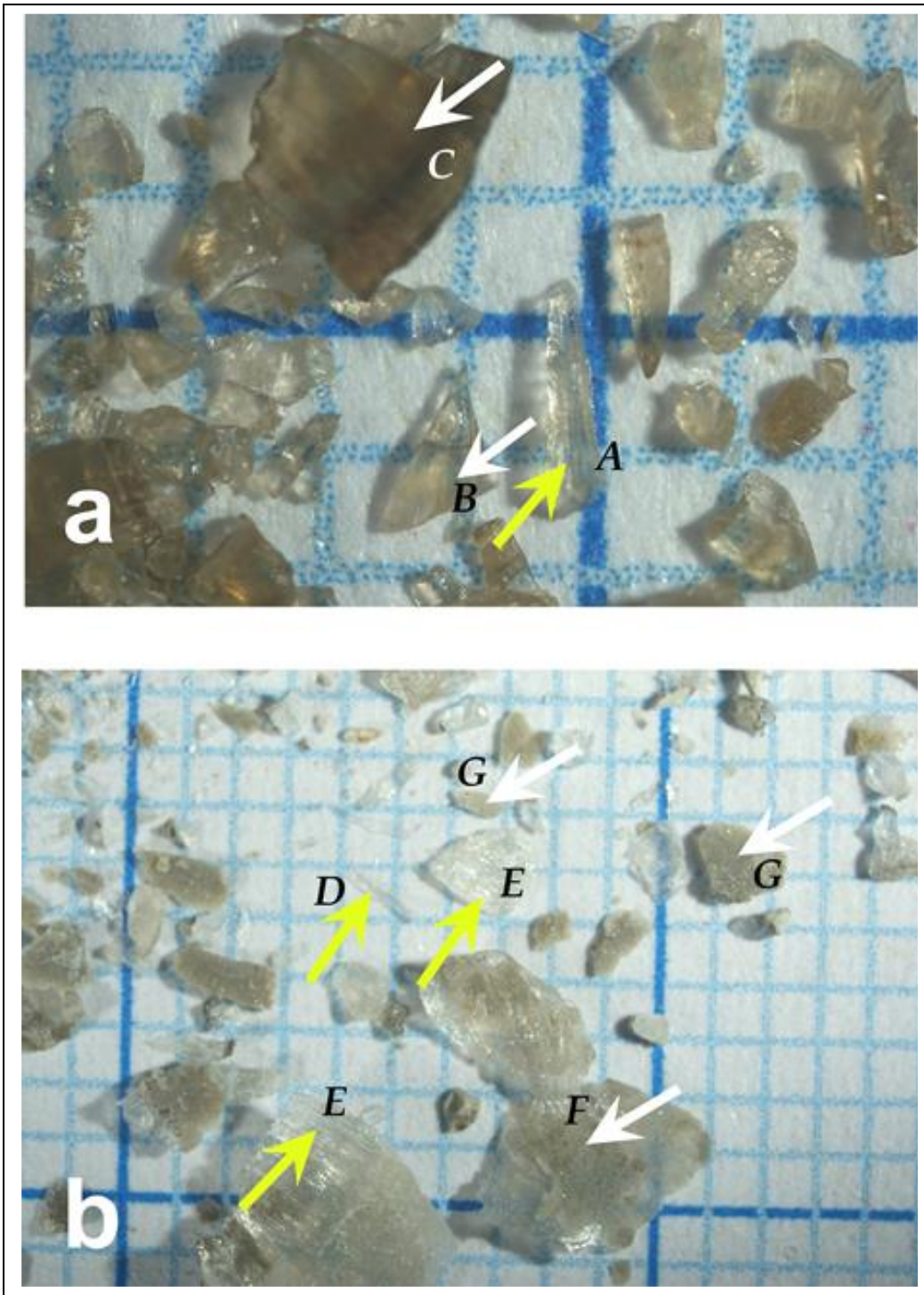

Fig. S1. Photomicrographs of fragments of a) a Peniche belemnite and b) brachiopod 9.65 m. White arrows point to altered fragments, yellow arrows point to unaltered fragments. Squares are 1 mm on a side. A, a fragment of pristine belemnite showing clear calcite with a strong radial fabric (oriented N-S); B, a triangular fragment in which pristine calcite (upper 30%) is separated from slightly altered calcite (lower 70%) by a black band that is interpreted to be organic matter. C, altered, cloudy, calcite from close to the belemnite exterior; useless for most chemical study. D, pristine crystallite of clear, pristine, calcite. E, foliated sheets of bundled crystallites of clear, pristine, calcite that flake to give thinner sheets and individual crystallites. F, foliated sheets of calcite in which the uppermost sheet is partly altered and cloudy. The upper sheet was easily flaked off from the underlying pristine calcite. G, altered calcite, the right-hand fragment being more altered than the left-hand fragment; both are useless for most chemical study.

44

the literature (*e.g.* Brand and Veizer 1980, 1981; Podlaha *et al.* 1998); the Ba concentrations are ≤ 17 ppm with only 3 samples > 6 ppm; these low concentrations indicate good preservation in the sub-samples analyzed. Concentrations of Mn are < 20 ppm excepting one sample containing 43 ppm and Fe concentrations exceed 100 ppm in only two samples; these higher Fe and Mn concentrations can be attributed to oxides deposited on crystal surfaces rather than incorporation into the calcite structure on alteration.

Correlation of C and O isotopes in samples

The positive correlation between base-$\delta^{44/40}Ca_{cal}$ and temperature (Fig. 3a) might be interpreted as suggesting that isotope fractionation of oxygen into belemnites is controlled by kinetic isotope fractionation, not equilibrium isotope fractionation (McConnaughey 1989; Watkins *et al.* 2013; Daëron *et al.* 2019). Values of $\delta^{18}O$ do not correlate with $\delta^{13}C$ (Fig. S2, below) in any of our taxa, or within the combined group as a whole, as might occur were kinetic isotope-effects influencing oxygen isotope compositions (see also Uchikawa and Zeebe 2012). Furthermore, using paired clumped-isotopes, Bajnai *et al.* (2020) report equilibrium fractionation of oxygen isotopes into a belemnite (and by analogy, all belemnites?). In view of the above, we discount kinetic isotope fractionation as a significant factor in contributing to the scatter in the $\delta^{18}O$ data plotted in Fig. 3a.

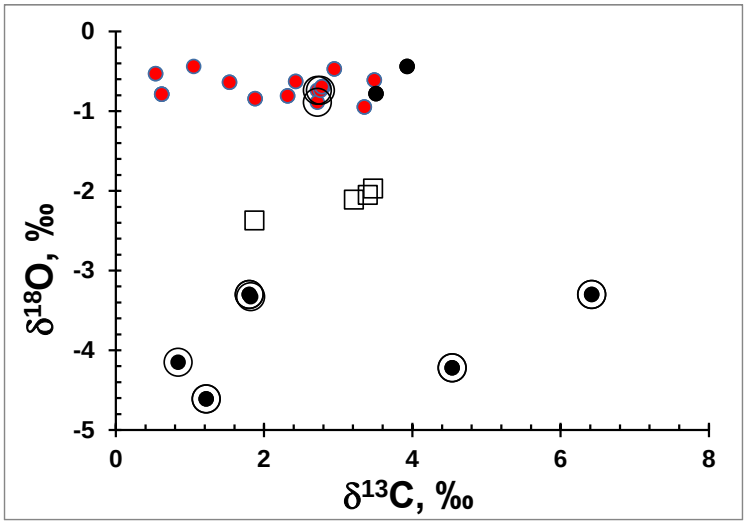

Fig. S2. Cross-plot of $\delta^{13}C$ *v* $\delta^{18}O$ for belemnites and brachiopods from Peniche, showing no relation between or within taxonomic groups

Analytical Methods.

Ca isotope methodology on Triton plus TIMS at Cambridge.

Samples of a few hundred micrograms were dissolved in 6M HNO_3 to make solutions with a Ca concentration of 1 µg/µl. Aliquots of 4 µl Ca were spiked with a ^{42}Ca – ^{48}Ca double spike, brought to dryness and then redissolved in 1 µl of 2M nitric acid for loading with H_3PO_4 as an activator on a double Re-filament assembly.

Measurements were done in two steps: ^{40}Ca to ^{44}Ca, and ^{42}Ca to ^{48}Ca. Masses of ^{40}Ca, ^{42}Ca, ^{43}Ca and ^{44}Ca were measured in the first sequence and ^{42}Ca, ^{44}Ca and ^{48}Ca in the second sequence (Table S1). Cup configurations are given in Table S2. The signal from ^{41}K was below 1mV so no correction for ^{40}K was required. The ^{40}Ca signal was constrained to a 0.5 – 1 nA window using a 10^{11} Ω resistor on collector L3. Each sample run consists of 10 blocks of 20 cycles each (for more detail of the the running protocol see Bradbury, 2018). Replicate measurements of NIST SRM-915b standard yield an average of 0.76 ± 0.12 ‰ (2sd, n = 29) on $\delta^{44/40}Ca$, relative to SRM-915a.

Table S1. Cup configuration for Ca isotope measurements on the Triton plus TIMS at Cambridge.

CUPS	**L4**	**L3**	**L2**	**L1**	**C**	**H1**	**H2**	**H3**	**H4**
STEP 1		^{40}Ca	^{41}K		^{42}Ca	^{43}Ca	^{44}Ca		
STEP 2	^{42}Ca			^{44}Ca					^{48}Ca

Ca isotopic analysis on IsotopX Phoenix-X62 TIMS at Royal Holloway

Sample were dissolved in 6M HNO_3 to make solutions with a Ca concentration of 1 µg/µl. Aliquots of 1 – 2 µl were loaded onto a single Re-filament in nitrate with TaF_5- H_3PO_4 emitter with the aid of parafilm dams to minimize sample spread. A ^{43}Ca – ^{46}Ca double spike was used to correct for mass fractionation. Isotopic abundances of Ca were measured in a static mode in one sequence shown in Table S2. Neither $^{87}Sr^{2+}$ nor Ti ions were observed in our samples. Running the Sr standard SRM987 whilst monitoring masses 40 – 44 detected no interference from Sr. Interference on ^{40}Ca from ^{40}K was monitored by measuring mass 41 and using the $^{40}K/^{41}K$ ratio of 0.0017384 for correction, but the ^{40}K correction was only 1 – 2 ppm.

With a Ca load of 1 – 2 µg, the ^{40}Ca signal was constrained to a 1.5 – 2 nA window using a $10^{10}\Omega$ resistor on collector L7. Each sample run contains 20 blocks, 10 cycles each, with 10 s integration time for each peak. Baselines were measured at half masses with 10 s integration time before and after each peak. The measured isotopic ratios of unspiked Ca isotopic standard HPSnew were then normalized to a $^{42}Ca/^{44}Ca$ of 0.30886 (Jorg *et al.* 2012). Analyses of unspiked HPS_{new} yielded mean values of 46.134855 ± 0.00096 (2se) for $^{40}Ca/^{44}Ca$, 0.064519 ± 0.00001 (2se) for $^{43}Ca/^{44}Ca$, and 0.001528 ± 0.00001 (2se) for $^{46}Ca/^{44}Ca$. and a mean $\delta^{44/40}Ca$ value of 0.71 ± 0.20 ‰ (2 s.d. n = 11) relative to SRM-915a, consistent with its published values (Reynard et al., 2010 and Li et al., 2016).

Table S2. Cup configuration for Ca isotope measurements on the Phoenix at RHUL

CUPS	L7	L4	L3	L2	AX	H1	H2	H3	H4
MASS	^{40}Ca		^{41}K	^{42}Ca	^{43}Ca	$^{87}Sr^{2+}$	^{44}Ca		^{46}Ca

The ^{43}Ca – ^{46}Ca double spike (DS) solution was made from stocks of OakRidge ^{43}Ca and ^{46}Ca spikes. Its calibrated isotopic compositions are listed in Table S3 and the concentration of each isotope in the DS was 1ng/g. Routinely, 1 µg of Ca in a sample was mixed with 10 µl of ^{43}Ca-^{46}Ca DS. Measured Ca-isotopic ratios of sample-spike mixtures were corrected offline for mass fractionation using a Matlab model (see Li *et al.*, 2016)

Table S3: Ca isotopic ratios and abundance of ^{43}Ca–^{46}Ca double spike (DS) solution; the isotopic abundances were calculated from the masses of each spike in the DS solution and their certified values of abundance.

Isotopic ratios	43-46Ca DS		Isotopic abundance* (%)	43-46Ca DS
$^{40}Ca/^{44}Ca$	9.256967 ± 0.000668		^{40}Ca	45.47
$^{42}Ca/^{44}Ca$	0.136588 ± 0.000005		^{42}Ca	0.77
$^{43}Ca/^{44}Ca$	4.328696 ± 0.000075		^{43}Ca	25.46
$^{46}Ca/^{44}Ca$	4.470016 ± 0.000151		^{44}Ca	5.50
			^{46}Ca	21.57
			^{48}Ca	1.18

S3. Sr isotope method

Samples were dissolved in sub-boiled 8 M HNO_3, purified using Sr-Spec resin, and loaded as nitrate on a single Re filament with TaF_5 - H_3PO_4 emitter. An ^{87}Sr - ^{84}Sr double spike solution was used to correct for mass fractionation and to determine the true Sr isotope ratios of samples. For isotopic measurement, the machine was run in multi-dynamic mode with correction for ^{87}Rb. Spiked and unspiked samples were prepared and run separately for $\delta^{88/86}Sr$ and $^{87}Sr/^{86}Sr$ analysis. A ^{87}Sr – ^{84}Sr spike solution was prepared from two single isotopically enriched Sr-carbonates (^{87}Sr-spike, ^{84}Sr-spike) from Oak Ridge National Laboratory (ORNL). The two carbonates were mixed to contain 43.5 % of ^{87}Sr spike solution and 56.5 % of ^{84}Sr spike solution, giving a $^{87}Sr/^{84}Sr$ ratio (0.87344) close to the optimum value of 0.8139 from the double spike inversion theory of Rudge *et al.* (2009) for similar ORNL ^{87}Sr – ^{84}Sr double spikes. The purpose was to optimize the effect of double spike and minimize the propagated errors on mass-fractionation corrected Sr isotope ratios.

The true Sr isotopic composition of the double spike solution was determined from the certified isotopic ratios of Sr standard SRM-987 and the measured ratios of ^{87}Sr – ^{84}Sr DS and SRM-987 – DS mixtures, by treating the ^{87}Sr – ^{84}Sr DS as the 'unknown' and the SRM-987 standard as the 'spike'. Data correction closely followed the Pb DS algorithm developed by Thirlwall (2000). The defined isotopic composition and isotope abundance (calculated) of the ^{87}Sr – ^{84}Sr spike solution are shown in Table S4.

Table S4: Sr isotopic ratios and abundance of $^{84\text{-}87}Sr$ double spike (DS) solution

Isotopic ratios	**84-87Sr DS**		**Isotopic abundance* (%)**	**84-87Sr DS**
$^{84}Sr/^{86}Sr$	15.80030		^{84}Sr	46.47
$^{87}Sr/^{86}Sr$	13.80063		^{86}Sr	2.45
$^{88}Sr/^{86}Sr$	3.83797		^{87}Sr	40.58
$^{87}Sr/^{84}Sr$	0.87344		^{88}Sr	10.50

Sensitivity Analysis for Variations in Salinity and $\delta^{18}O$.

The profiles of $\delta^{44/40}Ca$ against stratigraphic level (Fig. 5) show a positive excursion in Interval 2. The excursion occurs in raw data and in data corrected for temperature using a value of $\delta^{18}O_{sw}$ = −1 ‰. Here we show in Fig. S3 the effect of varying $\delta^{18}O_{sw}$ between +1‰ and −2‰ for seawater in Yorkshire whilst maintaining a value of −1‰ for Peniche. Other values can be interpolated or extrapolated from these values. Whatever values are chosen, the positive excursion in $\delta^{44/40}Ca$ remains in Interval 2.

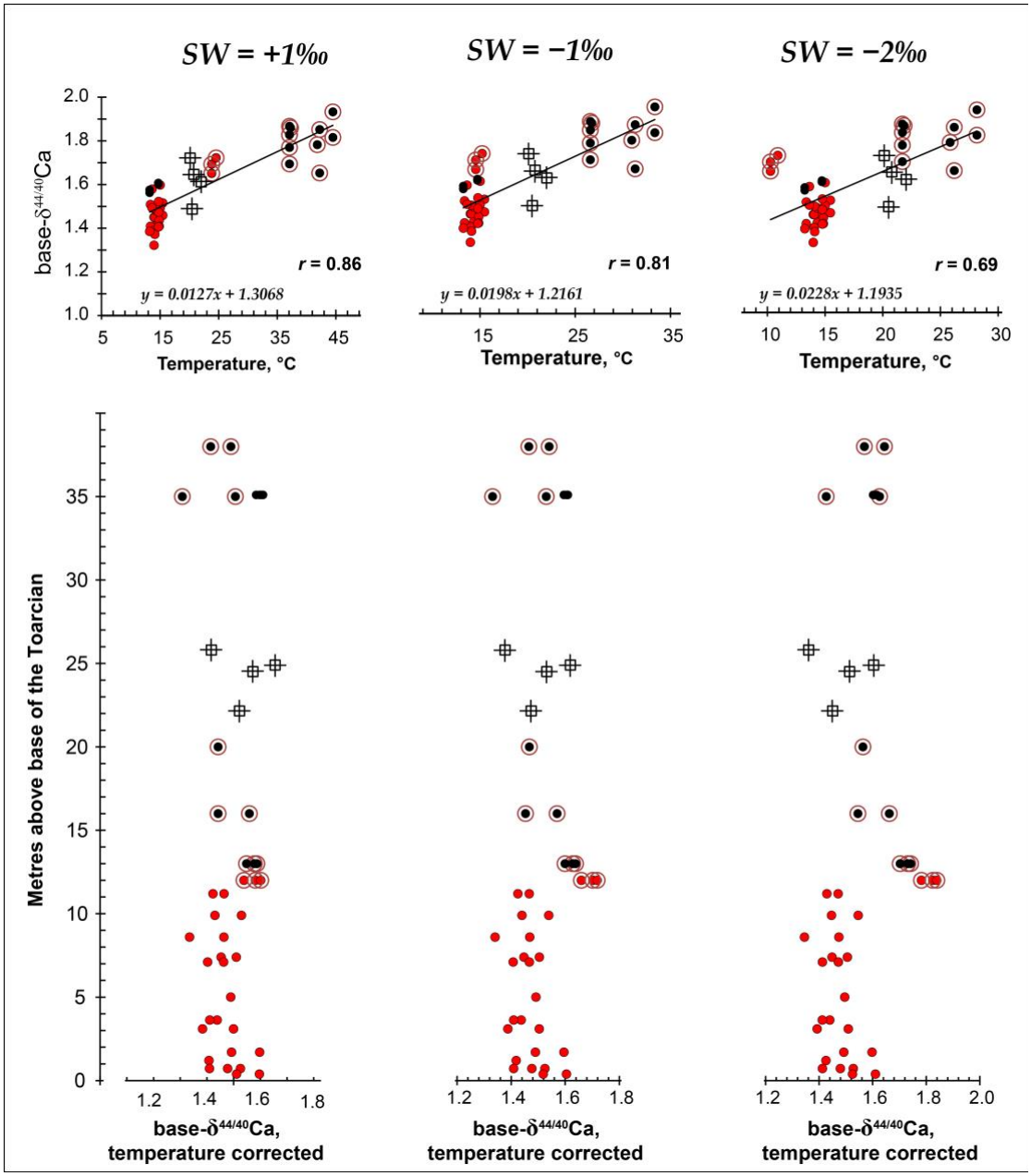

Fig. S3. Effect of differing values of $\delta^{18}O_{sw}$ on the temperature dependence of $\delta^{44/40}Ca$ (as shown in Fig. 3a (upper three diagrams) and on the stratigraphic profile of $\delta^{44/40}Ca$ as shown in Fig. 6 (lower three diagrams). Symbols as on previous figures.

Shown in Fig. S4a is a summary of the effect of varying $\delta^{18}O_{sw}$ between +2‰ and −3‰ for seawater in the *exaratum* Sz. whilst maintaining a value of −1‰ outside it. The maximum slope of the regression line is 0.0215. The maximum Pearson correlation coefficient is 0.86. Whatever values between −3‰ and +2‰ are chosen for $\delta^{18}O_{SW}$ in the *exaratum* Sz., the positive excursion in $\delta^{44/40}Ca$ remains in Interval 2 (Fig. S4b).

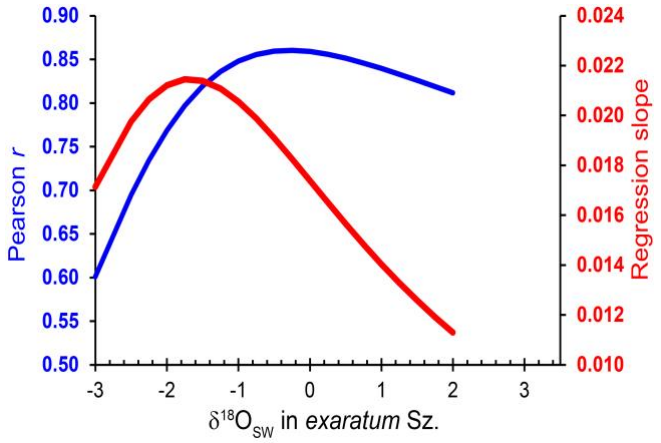

Fig. S4a. ***In blue***: the Pearson correlation coeffient between base-$^{44}Ca/^{40}Ca_{cal}$ and temperature (from $\delta^{18}O_{SW}$, see Fig. 3a), plotted as a function of $\delta^{18}O_{SW}$ in Interval 2, as $\delta^{18}O_{SW}$ outside the interval is held at −1‰. ***In red***, the regression slope for the correlation between base-$^{44}Ca/^{40}Ca$ and temperature (from $\delta^{18}O_{SW}$, see Fig. 3a), plotted as a function of $\delta^{18}O_{SW}$ in Interval 2 as $\delta^{18}O_{SW}$ outside it is held at −1‰

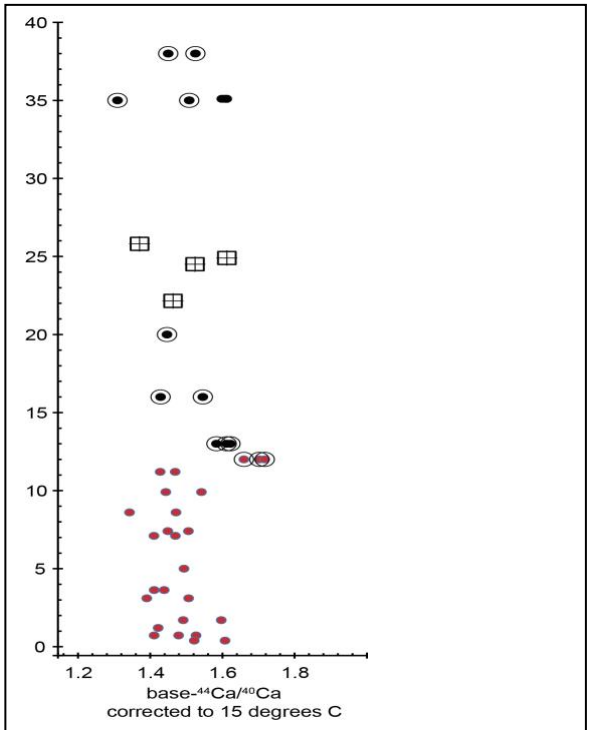

Fig. 4b. Profile of $^{44}Ca/^{40}Ca$, temperature correction with a maximum coefficient of 0.0215 ‰/°C,not the 0.020 used in Fig. 3a.

Combined models of Silva Tamayo et al. (2015)

In Fig. S5 we show the isotopic profiles that result from combining the models of Silva-Tamayo *et al*. (2015). The combined profiles do not match our measured profiles.

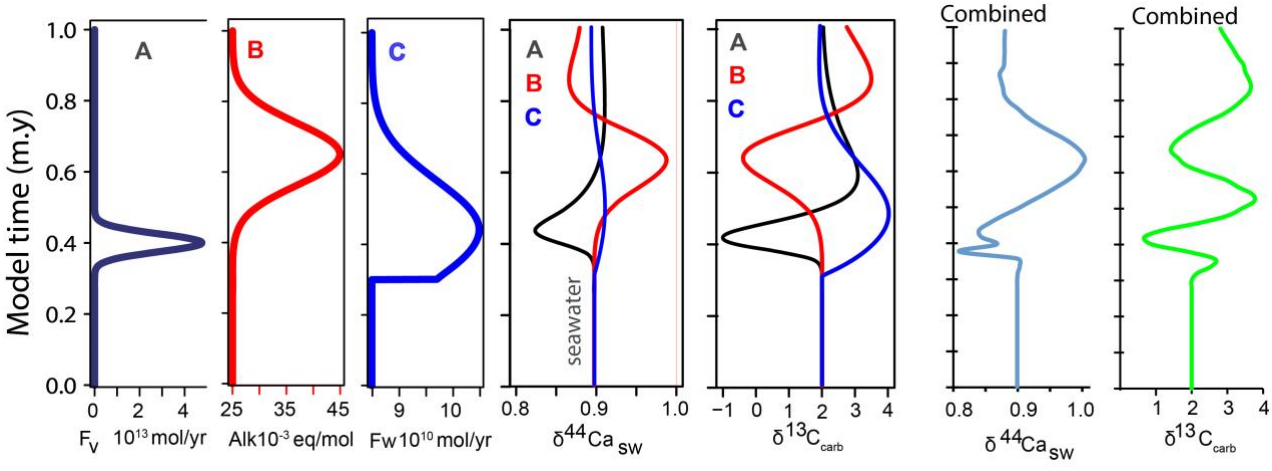

Fig. S5. Forcing functions (LHS) used in the model of Silva-Tamayo *et al.* (2018), the individual responses on two plots (centre) and the combined responses (RHS). None of the responses provides the linear, unchanging, profiles we report for $^{44}Ca/^{40}Ca$ or $^{88}Sr/^{86}Sr$.

Data of Müller *et al.* (2020), M20 hereinafter.

Muller et al. (2020) report profiles through Peniche of $\delta^{11}B$ and interpret them as showing ocean acidification in correlative equivalent of the *exaratum* Sz. Here we examine the robustness of the data on which that conclusion is based.

Sample selection

A detailed curve of $\delta^{13}C$ in bulk sediment through the Peniche section was provided by Hesselbo *et al.* (2007), who showed that belemnite $\delta^{13}C$ closely tracked bulk-sediment $\delta^{13}C$ but was offset to higher values by 0 to 1.5% ‰. Similar tracking and offsets were found by McArthur *et al.* (2020) for belemnites, by Suan *et al.* 2008 for brachiopods. Of the brachiopods of M20, all but P48, at 17.42 m above datum, track bulk carbonate. Sample P48 (arrowed in Fig. S6) has a $\delta^{13}C$ value of +3.18 ‰, which is too for its stratigraphic position. The value is 3.42‰ heavier than sample P49, at 17.52 m, but was not analysed for $\delta^{11}B$. The stratigraphic position of P48 is incorrect, so its value of $\delta^{11}B$ should be discounted.

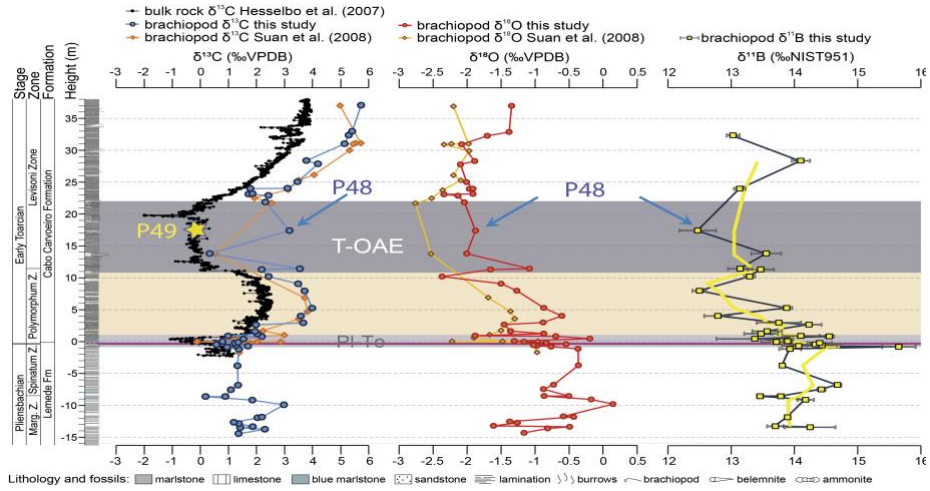

Fig. S6. Figure 1 of M20. The carbon-isotope value for P48 does not accord with its stratigraphic position. In the 'T-OAE' the $\delta^{13}C$ should be between 0 and +1‰. It is +3.4‰, so the sample should be disregarded.

Sample Preservation: Sr-isotopes.

The excessively high values of $^{87}Sr/^{86}Sr$ of all but two samples of M20 analysed for $^{87}Sr/^{86}Sr$, relative to expected values (Fig. S7), shows that the Sr-isotope system in almost all samples of M20 analysed for $^{87}Sr/^{86}Sr$ has been disturbed. It is unlikely that the Sr-isotope system has been disturbed whilst the B-isotope system has not, so the $\delta^{11}B$ values are suspect.

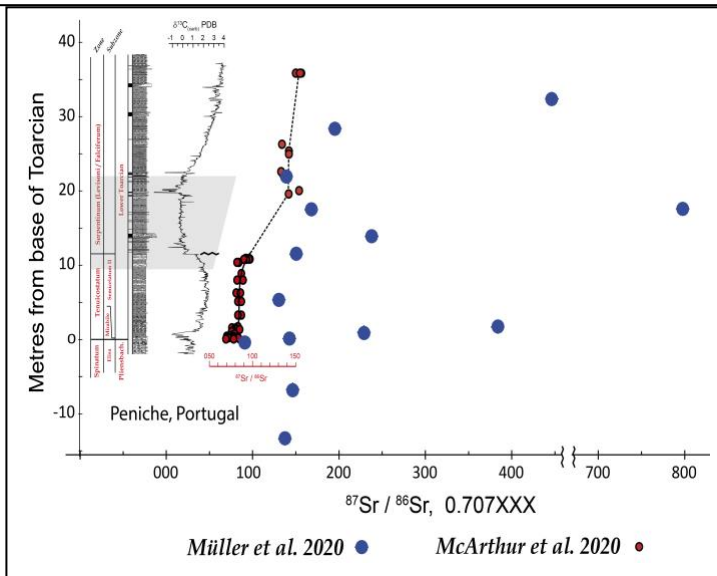

Fig. S7. Comparison of $^{87}Sr/^{86}Sr$ profiles for Peniche from M20 and from McArthur *et al.* (2020); the former are higher by up to to 0.000 650 and so plainly altered.

Sample preservation: aluminium concentrations

The samples of M20 contain up to 4.1 % of Al (Supplementary Information of M20) and correlate with concentrations of Mg (Fig. S8). The correlation shows the presence of a contaminant phase with a Mg/Al mass-ratio of 0.75. The Mg/Al mass ratio of 0.75 is within the wide range reported for diagenetic palygorskite. The presence of such a contaminant phase (or others that are unidentified) provides a ready explanation of why $^{87}Sr/^{86}Sr$ values of many samples are so high – they are reflecting not just Sr in biogenic calcite but also Sr in contaminant Al-rich phases.

It is therefore no surprise that concentrations of Al correlate with $\delta^{11}B$ (Fig. S9).

To find useable data in M20, there are two ways to filter out samples that appear altered. Firstly, by discarding samples with aberrant $^{87}Sr/^{86}Sr$. Secondly, by duiscarding all samples with Al concentrations > 1000. Doing both is, perhaps preferable and leaves no samples between 0 and 22 m in the section, making it impossible to identify any trend in the critical Interval 2 (Fig. S10).

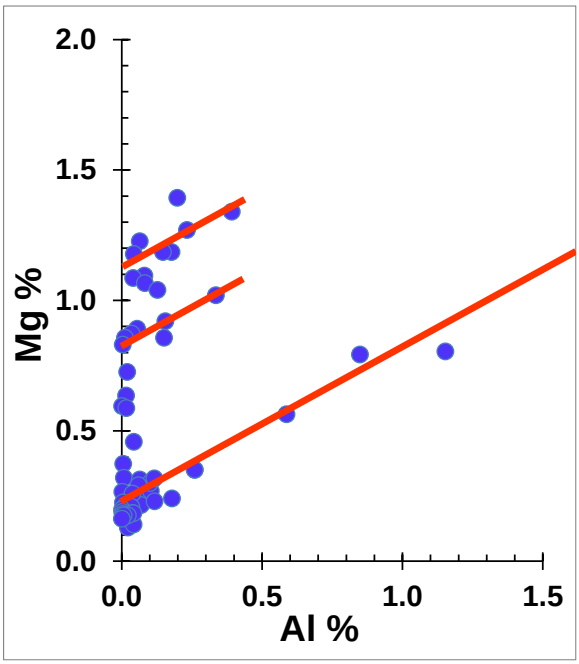

Fig. S8. Al *v* Mg in samples analysed by M20 for $\delta^{11}B$. Red squares are samples for which Mg and Al correlated strongly. Two samples not shown contain 2.1 % and 4.1 % Al and fall on the lowest red correlation line but were not used by M20 for pH-reconstruction.

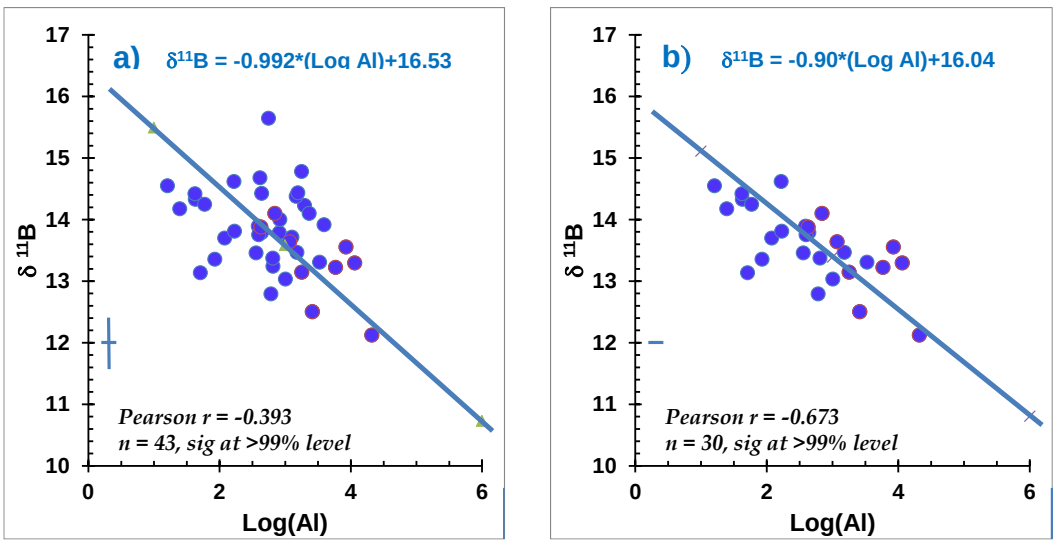

Fig. S9. Relation of Al to $\delta^{11}B$ in the data of M20. **a)** all data; b) excluding *Liospiriferina*

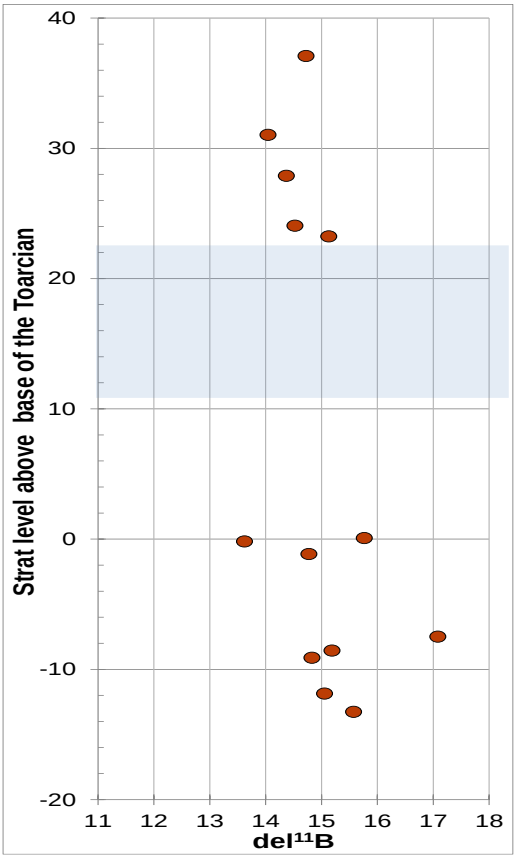

Fig. S10. Plot of $\delta^{11}B$ against stratigraphic level for samples with < 1000 ppm B and good $^{87}Sr/^{86}Sr$ values. The *exaratum* Sz is shaded in light blue.

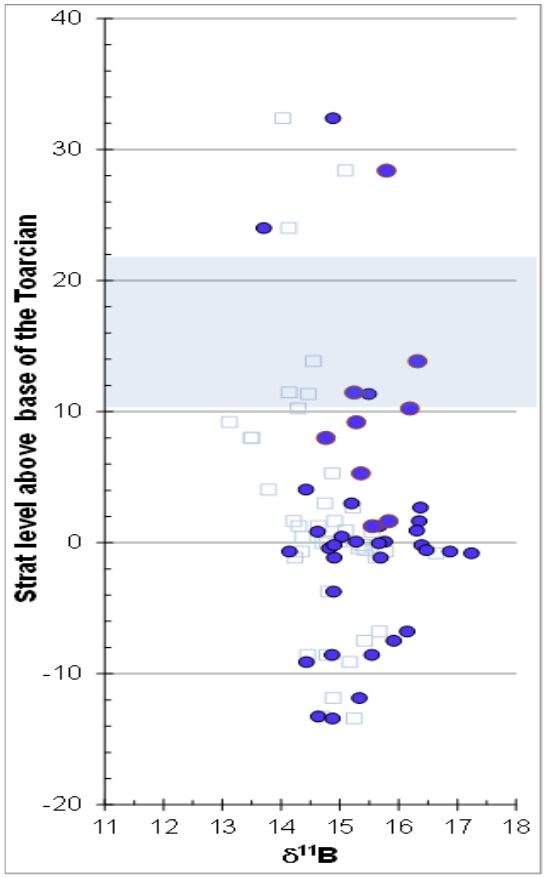

Fig. S11. Profiles of $\delta^{11}B$ in brachiopod calcite from Peniche; data of M20 corrected for Al contamination (blue filled circles; see text). Feint open squares are original data of M20 not corrected for Al contamination. Blue vertical lines is drawn at the mean values of corrected $\delta^{11}B$, with a width equal to analytical uncertainty, calculated as a mean deviation from the means of 10 analyses of 5 pairs of samples from 5 different stratigraphic levels (mean = 0.39 ‰, 2 s.d. = 0.58‰ , n = 5).

An alternative to discarding altered samples is to correct for the effect of Al-contamination on $\delta^{11}B$ using the correlation between Al concentrations and $\delta^{11}B$ (Fig. S9a). In practice, some caution is needed in doing so. Firstly, the correlation line in Fig. S9a extrapolates to a value of around 11.5‰ for $\delta^{11}B$ at 10^5 µg/g of Al, which is approximating 100% Al-bearing contaminant. Marine clays typically have negative $\delta^{11}B$. The slope of the correlation line is therefore less than expected were the contamination to be due to the presence of detrital clay, a consideration that strengthens our view that the contamination reflects precipitation of Al in diagenetic palygorskite.

Whatever the contaminant phase(s), its influence on samples will depend on the relative concentrations of B in contaminant and sample and their respective $\delta^{11}B$. Alteration will have more effect on samples with low concentrations of B (*e.g. Soaresirhynchia*, 11 to 36 µg/g) than on samples with high concentrations (*Liosiriferina*; 743 to 1585 µg/g). Indeed, it might be that the concentrations of B in *Liospiriferina* are too high to be much altered by diagenesis.

To accommodate this observation, and refine the possible influence of alteration on $\delta^{11}B$, we show in Fig. S9b samples without *Liospififerina*, an exclusion that improves the correlation of Al with

$\delta^{11}B$. Nevertheless, we show in Fig. S11 the stratigraphic profile of $\delta^{11}B$ corrected using the relationship shown in Fig. S9a; there appears to be no unequivocal change in $\delta^{11}B$ through the interval studied so, we conclude, there is no evidence for ocean acidification in the $\delta^{11}B$

Sample preservation: relation to $\delta^{18}O$

M20 note that, through the section, "*The changes in $\delta^{11}B$ closely follow the $\delta^{18}O$ record (r = 0.75, p <0.0001.)….*". A correlation is confirmed by a cross-plot of $\delta^{18}O$ and $\delta^{11}B$ (Fig. S12), but the correlation is barely significant (90% level) when all samples are included (Fig. S10a). It is significant at the 99% level when *Liospiriferina* is omitted from the plot (Fig. S12b).

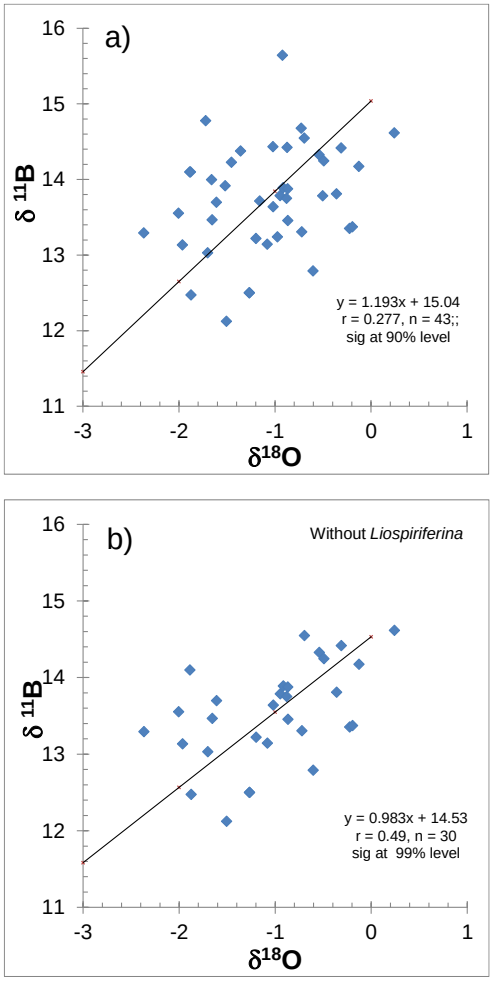

Fig. S12. Relation of $\delta^{11}B$ to $\delta^{18}O$ in samples of M20. a) all samples; b) excluding *Liospiriferina*.

Penman *et al.* (2013) noted a positive relation in brachiopods between $\delta^{11}B$ and $\delta^{18}O$, with $\delta^{11}B/\delta^{18}O$ between 1.4 and 2.4. In Fig. S12 the values are 1.2 and 1.0. The relationships suggest that the incorporation of B isotopes into brachiopod calcite is controlled, in part, by vital effects, and/or the temperature and/or the rate of calcification.

Penman *et al.* (2013) also noted that in brachiopods "*intra-shell variability up to 7‰ was observed in $\delta^{13}C$ and $\delta^{18}O$ possibly because of kinetic isotope fractionation effects (Carpenter and Lohmann, 1995; Auclair et al., 2003)…*". Only for M20's brachiopod species *Soaresirhynchia* do $\delta^{13}C$ and $\delta^{18}O$ correlate well (orange open circles on Fig. S13), suggesting either alteration, or a kinetic effect on $\delta^{13}C$ and $\delta^{18}O$ for this species. A rate effect on $\delta^{11}B$ may therefore affect *Soaresirhynchia*.

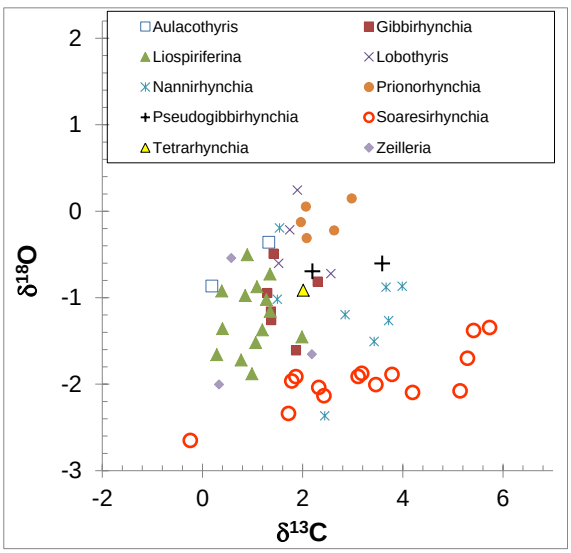

Fig. S13. Relation of $\delta^{13}C$ to $\delta^{18}O$ in brachiopods. Only *Soaresirhynchia* (orange open circles) shows a correlation between the two.

Species bias.

Penman *et al.* (2013), in summarising previous work on $\delta^{11}B$ brachiopods, noted that "*Boron isotope data from various modern species of brachiopods exhibit a large (15–23‰) range (Hemming and Hanson, 1992; Lécuyer et al., 2002; Joachimski et al., 2005; Simon et al., 2006), which is too great to be attributed solely to regional pH variations.*".

Such observations undermine attempts to use brachiopods for pH reconstruction. We speculate that the large spread in the data of M20 for any particular stratigraphic level arises both from alteration and from species differences in values of $\delta^{11}B$. For example, samples P22 and P23, both recovered from a position 71 cm below the Pl-Toa boundary, have values that differ by 1.43 ‰ (*Liospiriferina rostrata* = 14.78 ‰; *Prionorhynchia serrata* = 13.35 ‰).

Intra-species variation

Jurikova *et al.* 2019, noted that *"...boron incorporation into the innermost shell layers* (of brachiopods) *is primarily driven by calcifying fluid pH, whereas the outermost calcite layers are to some extent influenced by ambient seawater pH.*". Such an observation accords with the notion that the outer (primary) shell of brachiopods is deposited out of equilibrium with ambient seawater whilst the inner (secondary) shell approaches isotopic equilibrium (Carpenter and Lohmann 1995). This view is confirmed by Bajnai *et al.* (2018) for brachiopods. Non-equilibrium precipitation of calcite is seen in the range of 3.5 ‰ range in $\delta^{11}B$ across individual brachiopod shells reported by Penman *et al.* (2013) and in the correlation of values of $\delta^{11}B$ with $\delta^{18}O$ in brachiopod shells (*ibid.*). It is not certain that such influences are absent in the subsamples of M20.

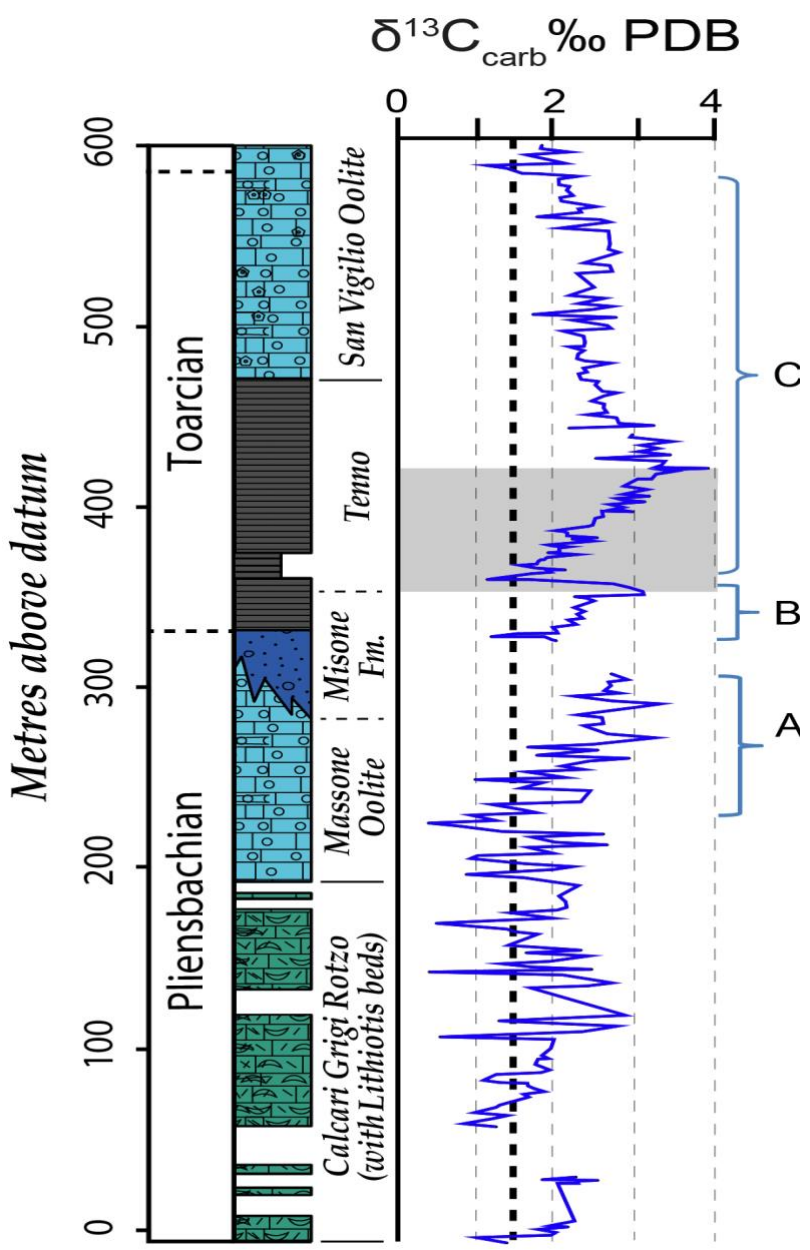

Fig. S14. Trend of $\delta^{13}C_{carb}$ through the Trento Platform, after Ettinger *et al.* (2021). Grey area denotes the putative T-OAE as it is identified by those authors. Between A and B, and between B and C, values of $\delta^{13}C_{carb}$ return to around +1‰ to +2‰, which are interpreted as typical (background) values for early Mesozoic times. Heavy dashed line drawn at +1.5 ‰ .

Positive excursions are labeled A, B, C. Positive excursion B is the *Tenuicostatum* Zone positive excursion noted by many authors. Positive excursion C is truncated in many C-isotope profiles. The failure to define the C-isotope stratigraphy over the full stratigraphic profile show here has lead many to the erroneous interpretation that the return to backgrounds are negative isotope excursions.

Completeness of the Section at Peniche and Age Model of M20.

The Peniche Section is the GSSP for the Toarcian. The rules for adoption of a GSSP are set out one https://stratigraphy.org/gssps/ (accessed on 10/09 2020). The Peniche section contravenes rules 4, 7 and 8, which are :

4. ***The horizon in which the marker appears should have minerals that can be radiometrically dated.***
7. ***The outcrop has to have an adequate thickness.***
8. ***Sedimentation has to be continuous without any changes in facies***

The Pl-To boundary interval at Peniche is marked by a hardground (Rocha *et al.* 2016). The boundary shows extreme condensation and the Tenuicostatum Zone is an interval of varying sedimentation rate (McArthur *et al.* 2020a). These facts compromise the age model developed for the interval by Müller *et al.* (2020), which is based on a cyclostratigraphic analysis of Peniche that ignores these observations. To emphasise this point, we reproduce the following from McArthur *et al.* (2020), together with Fig. 4 of those authors shown here as Fig. S12.

At Peniche, values of $^{87}Sr/^{86}Sr$ increase by 0.000 012 over the first 3 metres of section (Fig. 3) and then remain at 0.707 085 over the next 2.5 m (to 5.5 m). Upsection from 5.5 m to 11.1 m, the rate of increase in 87Sr/86Sr increases as level increases. It follows that the sedimentation rate through the Tenuicostatum Chronozone was lowest in the basal 3 m of the section, highest between 3 and 5.5 m, where 87Sr/86Sr remains constant, and decreased upward from 5.5 m to the base of the Serpentinum Chronozone at 11.1 m. Of the increase in $^{87}Sr/^{86}Sr$ of 0.000 023 though this chronozone, half occurs in the basal 3 m of the section, so half of Tenuicostatum time is compressed (non-linearly) into this basal 3 m of section. Most of the rest of Tenuicostatum time is non-linearly recorded in the sediments between 5.5 and 11.1 m. These observations of varying sedimentation rates will affect any cyclostratigraphic interpretation of the section (Suan et al. 2008b, Huang and Hesselbo 2014, cf. Ruebsam et al. 2014) …

That the sedimentation rate was slowest in the basal 3 m of the section is no surprise: Elmi (2007) noted that Bed 15 is a "condensed interval" and that characteristics of the 5 beds in Bed 15a–15e "indicate a low sedimentation rate" and also that these beds "are capped by a hard ground (top surface of level 15e in Mouterde 1955…)". Our Sr-isotope data show that this condensation extends into the overlying 3 m of sediment with condensation intensity decreasing upwards. Condensation is confirmed by the relative thicknesses of the Mirabile and Semicelatum II Subchronozones at Peniche compared to elsewhere (Fig. 4). ……..

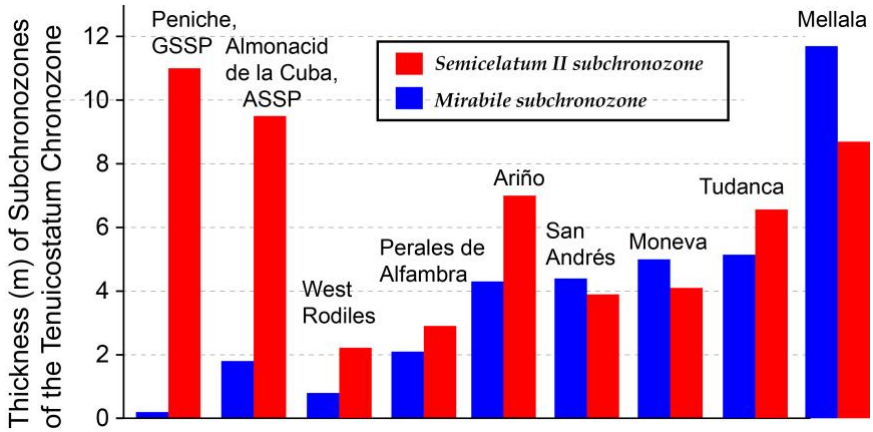

Fig. S15. Reproduction of Fig. 4 of McArthur *et al.* 2020, showing the extreme condensation across the boundary interval at Peniche.

To further illustrate the point that the age model of Muller et al. (2019) is inaccurate, we note that it is based on the cyclostratigraphic analysis of the Peniche section by Huang and Hesselbo (2014) who, in undertaking that analysis, made inadequate allowance for changes in sedimentation rate through the interval. According to Huang and Hesselbo (2014), " a duration of ~58 kyr was estimated for the negative $\delta^{13}C_{carb}$ excursion at the Pliensbachian/Toarcian boundary from the 405-kyr tuned series (Fig. 3D), although we note … a degree of stratigraphic condensation within about a meter on either side of the boundary (Elmi, 2006), meaning that the estimate should be considered a minimum.".

Three problems arise with this cyclostratigraphical estimate. Firstly, the data were 'detrended' and this procedure introduces spurious spectal peaks in cyclostratigraphic analysis (Vaughan et al. 2015). Secondly, the minimum isn't at the boundary, but some 0.7 m above it in a highly condensed section in which stratal thickness does not equate to time. Thirdly, the negative $\delta^{13}C_{carb}$ excursion includes the mirabile Subzone (0–0.2 m above the boundary), and some 0.68 m of the overlying, condensed, part of the semicelatum II Subzone, which is 11 m thick. The negative excursion in $\delta^{13}C_{carb}$ therefore occupies all of mirabile time and a minimum of 0.68/11 of semicelatum II time (and probably more, given the condensation noted here and by Huang and Hesselbo, 2014). Given the relative thicknesses (and so roughly, durations) of these two subzones elsewhere than Peniche (Fig. 4 of McArthur et al. 2020) the duration of the negative excursion in del^{13}Ccarb cannot be, as they state "~58 ka". This estimate has a nock-on effect on estimates of the duration of other parts of the section which, in turn, cannot be correct.

Additional References

Bajnai D., Guo W., Spötl C., Coplen T.B., Methner K., Löffler N., Krsnik E., Gischler E., Hansen M., Henkel D., Price G.D., Raddatz J., Scholz D. and Fiebig J. 2020. Dual clumped isotope thermometry resolves kinetic biases in carbonate formation temperatures. Nature Communications, 11:4005, https://doi.org/10.1038/s41467-020-17501-0.

Bajnai D., Fiebig J., Tomašových A., Garcia S.M., Rollion-Bard C., Raddatz J., Löffler N., Primo-Ramos C. and Brand U. 2018. Assessing kinetic fractionation in brachiopod calcite using clumped isotopes. Scientific Reports, 8:533. DOI:10.1038/s41598-017-17353-7

Brand U. and Veizer J. 1980. Chemical diagenesis of a multicomponent carbonate system: 1. Trace elements. *J. Sediment. Petrol.* 50, 1219–1236.

Brand U. and Veizer J. 1981. Chemical diagenesis of a multicomponent carbonate system: 2. Stable isotopes. *J. Sediment. Petrol.* 51, 987–997.

Carpenter S.J. and Lohmann K.C. 1995. $\delta^{18}O$ and $\delta^{13}C$ values of modern brachiopod shells. Geochimica et Cosmochimica Acta, 59 (18) 3749-3764.

Jurikova H., Liebetrau V., Gutjahr M., Rollion-Bard C., Huc M.Y., Krause S., Henkel D., Hiebenthal C., Schmidt M., Laudien J. and Eisenhauer A. 2019. Boron isotope systematics of cultured brachiopods: Response to acidification, vital effects and implications for palaeo-pH reconstruction. Geochimica et Cosmochimica Acta 248, 370–386.

Penman D.E., Hönisch B., Rasbury E.T., Hemming N.G., Spero H.J. (2013). Boron, carbon, and oxygen isotopic composition of brachiopod shells: Intra-shell variability, controls, and potential as a paleo-pH recorder. Chemical Geology, 340, 32–39.

Pittet, B., Suan, G., Lenoir, F., Duarte, L. V., Mattioli, L. V., 2014. Carbon isotope evidence for sedimentary discontinuities in the lower Toarcian of the Lusitanian Basin (Portugal): Sea level change at the onset of the Oceanic Anoxic Event. Sed. Geol. 303, 1–14.

Podlaha, O.G., Mutterlose, J., and Veizer, J. 1998. Preservation of $\delta^{18}O$ and $\delta^{13}C$ in belemnite rostra from the Jurassic/Early Cretaceous successions. *American Journal of Science*, **298**, 324–347.

Saelen, G. 1989. Diagenesis and construction of the belemnite rostrum. *Palaeontology*, **34(4)**, 765–798.

Vaughan S., Bailey R.J. and Smith D.G. 2015. Cyclostratigraphy: data filtering as a source of spurious spectral peaks. *In* Smith D.G., Bailey R.J., Burgess P.M. & Fraser A.J. (eds) Strata and Time: Probing the Gaps in Our Understanding. Geological Society, London, Special Publication, 404, 151–156.